

Discriminating Types Ia and Ib polar stratospheric clouds in POAM satellite data

A. W. Strawa,¹ K. Drdla,¹ M. Fromm,² R. F. Pueschel,¹ K. W. Hoppel,³ E. V. Browell,⁴ P. Hamill,⁵ and David P. Dempsey⁶

Received 12 February 2001; revised 22 June 2001; accepted 25 June 2001; published 18 October 2002.

[1] A method for discriminating Types Ia and Ib Polar Stratospheric Clouds (PSCs) from Polar Ozone and Aerosol Measurement (POAM) satellite occultation measurements of aerosol extinction coefficient is described. The method has been validated by applying several statistical tests to the results and by using Differential Absorption Lidar (DIAL) and Ozone Lidar Experiment (OLEX) lidar observations made during Stratospheric Aerosol and Gas Experiment (SAGE) III Ozone Loss and Validation Experiment/Third European Stratospheric Experiment on Ozone II (SOLVE/THESEO 2000). Type Ia PSCs are believed to be composed of large nitric-acid-containing particles that will sediment out of the stratosphere, causing denitrification and facilitating ozone depletion. Type Ib PSCs are believed to be much smaller and will not sediment out of the stratosphere. Discriminating between these two types of PSCs is significant because it will permit a better understanding of ozone depletion today and predict the fate and effect of PSCs using the more continuous temporal coverage and larger areal coverage that can be obtained from satellites. The method is made possible by the character of POAM observations when plotted as normalized extinction versus wavelength dependence. As the extinction increases, observations of Types Ia and Ib PSCs bifurcate. This behavior is also observed in idealized simulations of the formation of Supercooled Ternary Solutions (STS) and nitric acid trihydrate (NAT) particles, which are believed to make up Types Ib and Ia PSCs, respectively. Analysis of POAM observations from the 1999/2000 Arctic winter using the PSC discrimination algorithm revealed that the number of PSC observations peaked in January. In November, December, and January, the ratio of Type Ia to Ib PSCs was about 3. In February and March, this ratio was about 0.3. The average altitude of Type Ia PSCs descended more than the Type Ib, especially in the spring where the Type Ia observations were 2–3 km below the Type Ib observations. This is consistent with observations of denitrification during the 1999/2000 winter. The PSC discrimination algorithm is applicable to previous winters in both hemispheres and will work with SAGE III observations as well. This will permit a more extensive study of the statistical significance of some features of the PSCs observed during the 1999/2000 Arctic winter. It is our belief that the present method of analyzing satellite data to discriminate Type I PSCs will be of great utility in the study of PSCs and ozone depletion. *INDEX TERMS:* 0320

Atmospheric Composition and Structure: Cloud physics and chemistry; 0305 Atmospheric Composition and Structure: Aerosols and particles (0345, 4801); 0360 Atmospheric Composition and Structure: Transmission and scattering of radiation; 3360 Meteorology and Atmospheric Dynamics: Remote sensing; *KEYWORDS:* Polar stratospheric clouds, Stratosphere, Ozone loss, Satellite measurement remote sensing, cloud properties

Citation: Strawa, A. W., K. Drdla, M. Fromm, R. F. Pueschel, K. W. Hoppel, E. V. Browell, P. Hamill, and D. P. Dempsey, Discriminating Types Ia and Ib polar stratospheric clouds in POAM satellite data, *J. Geophys. Res.*, 107(D20), 8291, doi:10.1029/2001JD000458, 2002.

¹NASA Ames Research Center, Atmospheric Physics Branch, Moffett Field, California, USA.

²Computational Physics, Inc., Springfield, Virginia, USA.

³Naval Research Laboratory, Washington, D.C., USA.

⁴NASA Langley Research Center, Hampton, Virginia, USA.

⁵Department of Physics, San Jose State University, San Jose, California, USA.

⁶Department of Meteorology, San Francisco State University, San Francisco, California, USA.

1. Introduction

[2] The chemistry of stratospheric ozone loss involves heterogeneous reactions on clouds of small particles called Polar Stratospheric Clouds (PSCs). The term PSC refers to several distinct categories of cloud differentiated by unique observable characteristics. After some of the first observations of PSCs by *McCormick et al.* [1982] using Stratospheric Aerosol Measurement (SAM) II data, *Turco et al.* [1989] first differentiated Types I and II PSCs. Type II PSCs are observed at temperatures below the ice frost point

(typically about 188 K at stratospheric conditions) and have characteristics generally consistent with water ice particles. At warmer temperatures, up to about 7 K above the ice frost point, Type I PSCs are observed. *Browell et al.* [1990] distinguished two classes of Type I PSCs, Ia and Ib, from Arctic lidar observation. Type Ib clouds are characterized by high values of lidar backscatter and low depolarization. These clouds appear to be consistent with small liquid particles probably composed of ternary solutions of $\text{H}_2\text{SO}_4/\text{HNO}_3/\text{H}_2\text{O}$ [Toon et al., 1990, 2000; Drdla et al., 1994]. Type Ia clouds are characterized by moderate lidar extinction and high depolarization. These characteristics are consistent with larger solid particles [Toon et al., 1990] that are assumed to be composed of nitric acid trihydrate or dihydrate (NAT or NAD, respectively) [Hanson and Mauersberger, 1988; Worsnop et al., 1993].

[3] Interest in PSCs is driven by their effect on the fate of active forms of chlorine, such as ClO, that react rapidly to destroy ozone. This occurs in two ways. First, PSCs provide surfaces for heterogeneous reactions that produce active forms of chlorine from inactive, reservoir species, such as HCl and ClONO₂. Second, larger PSC particles that contain nitric acid sediment, permanently removing nitric acid from the higher altitudes of the stratosphere. This denitrification allows chlorine to remain in its active state, increasing ozone loss. Despite their importance, the formation mechanism responsible for Type Ia PSCs is uncertain [Tolbert and Toon, 2001].

[4] Antarctic PSCs have similar characteristics to those observed in the Arctic. *Rosen et al.* [1993] found from balloon-borne measurements that aerosols in the Antarctic exhibit properties similar to those of the Arctic Types Ia and Ib. Airborne Southern Hemisphere Ozone Experiment (ASHOE) data show that high supersaturations are initially required to form NAT PSCs in the Antarctic just as they are in the Arctic [Dye et al., 1996; Del Negro et al., 1997]. *Santee et al.* [1999] show that nitric acid profiles in the Antarctic are consistent with several types of PSCs forming under differing temperature histories.

[5] In situ observations can provide evidence of episodic denitrification, but satellite observations are needed to show the full extent of denitrification. Denitrification is a widespread phenomenon in the Antarctic stratosphere [see, for example, *Santee et al.*, 1999]. Reports of denitrification in the Arctic are not as common. Balloon-borne studies show that denitrification and sedimentation of nitric acid in the lower stratosphere do occur in the Arctic [Schlager et al., 1990]. ER-2 measurements showed significant denitrification, suggesting that particle sedimentation removed nitrogen from the stratosphere during the Airborne Arctic Stratospheric Experiment (AASE) I [Fahey et al., 1990]. Recent satellite observations also show evidence for denitrification in the Arctic [Santee et al., 2000].

[6] One major result from the recent Stratospheric Aerosol and Gas Experiment (SAGE) III Ozone Loss and Validation Experiment and the Third European Stratospheric Experiment on Ozone II (SOLVE/THESEO 2000) is in situ evidence of the existence of very large ($D > 10 \mu\text{m}$) particles that contain nitric acid [Fahey, et al., 2001]. Concurrent lidar measurements confirm that these are Type Ia PSCs. The significance of this finding is that these large particles have appreciable sedimentation

velocities. As these large particles fall they take nitric acid out of the stratospheric regions, causing denitrification. Denitrification is the permanent loss of nitric acid from an atmospheric layer. Thus, denitrification leads to increased ozone loss by allowing chlorine to remain in its active forms (e.g., ClO) longer. Supercooled Ternary Solutions (STS) or Type Ib PSCs are smaller and sediment too slowly to cause severe denitrification to any appreciable degree. Thus it would be very important to be able to use satellite data to discriminate between Types Ia and Ib PSCs. One could potentially identify denitrification events and study the formation mechanisms of these types of PSCs over the longer time spans and larger area coverage available with satellites.

[7] This paper presents a method for discriminating Types Ia and Ib PSCs using the Naval Research Laboratory's Polar Ozone and Aerosol Measurement (POAM III) satellite occultation observations of aerosol extinction coefficient. The observations are described briefly. Then the algorithm and its theoretical basis are described in the next section. Lidar data are used to verify the method. Aspects of the extinction-wavelength dependence behavior of POAM observations are discussed. Finally, results of the method applied to the Arctic 1999/2000 winter are presented.

2. Observations

[8] The POAM III instrument is a visible/near infrared solar occultation photometer which measures stratospheric constituents in the polar regions of both hemispheres. POAM makes 14 to 15 measurements per day in each hemisphere around a circle of latitude between about 61° and 69° [Lucke et al., 1999]. First measurements were obtained in April 1998. The POAM III measurement complement includes ozone, water vapor, NO₂, and aerosol extinction. The wavelengths used for aerosol extinction are 0.3534, 0.4422, 0.603, 0.779, 0.9924, and 1.018 μm . This paper utilizes measurements made at 0.603 and 1.018 μm . For brevity, we refer to these wavelengths as 0.6 and 1 μm . The method for identification of PSC profiles (i.e., a POAM profile containing at least one PSC aerosol enhancement) is described by *Fromm et al.* [1997, 1999]. This method uses only enhancements in the 1 mm extinction. For analysis of individual PSC extinction measurements in this paper, we have used only PSCs with extinction coefficients that meet the 4-sigma PSC threshold [Fromm et al., 1997]. This restriction eliminates PSCs with low values of extinction coefficient. It is unlikely that these PSCs contain particles with enough mass to cause denitrification.

[9] The subject of this study is the Arctic winter of 1999/2000. The conditions during this winter were favorable for the formation of Type I PSCs. Additionally, the SOLVE/THESEO 2000 mission, conducted during this period, provided much useful information and valuable insights into Types Ia and Ib PSC formation and characteristics. As part of this study NASA Langley's differential absorption lidar (DIAL) [Browell et al., 1990] was flown on NASA's DC-8 from Kiruna, Sweden. Scattering ratios and aerosol depolarization were derived from the lidar measurements at 0.604 and 1.064 μm . Another lidar, the Ozone Lidar Experiment (OLEX) was flown aboard the DLR Falcon

during the international SOLVE/THESEO 2000 campaign at this same time [Dörnbrack *et al.*, 2002]. PSC type was determined using the criteria outlined by Browell *et al.* [1990]. These lidar measurements were used to validate the discrimination algorithm presented in this work.

[10] Aerosol radiative extinction was calculated using a Mie scattering code. The refractive index of sulfate solutions were taken from Steele and Hamill's [1981] fit to the Palmer and Williams [1975] data and those of ternary solutions based on weighted averages of binary solutions calculated by a routine provided by U. Krieger [Lou *et al.*, 1994]. The refractive index of water ice, SAT, and NAT was fixed at 1.33, 1.40, and 1.43, respectively, independent of wavelength and temperature. The imaginary component of all refractive indices was set to zero for the wavelengths under consideration. The calculation does incorporate the effect of cores in the particles (i.e., the SAT core inside a NAT particle). A comparison between extinctions calculated with this model and POAM II observations has been made by Steele *et al.* [1999]. Generally, changes in the refractive index in this range have a second order effect on the extinction when compared to changes in particle size and morphology. For instance, changing the refractive index for NAT from 1.4 to 1.35 changes the extinction by less than 1%.

[11] The Mie theory assumes a spherical particle shape and Type Ia PSCs are likely to be solid crystals. Mishchenko [1993] compared Mie calculations of spherical particles to calculations using the T-matrix method to calculate light scattering by size-shape distributions of axially symmetric particles. The applicability of the T-matrix technique for this application is discussed in this reference. His results showed that the extinction cross section was increased by only 10% in the worst case when various spheroids were used rather than spherical particles. Furthermore, the only information we have on the crystal habit of Type I PSC are from replicator data and the polarization of lidar signals. The lidar data indicate that the particles are not spherical. Replicator samples show a variety of shapes: hexagonal plates, columns, triangles, and amorphous shapes [Goodman *et al.*, 1997]. Thus it is difficult to know what shape and orientation to assume for the radiative calculations. As part of our future work, we plan to carry out some calculations to determine the wavelength dependence of the extinction coefficient with particle shape.

3. The PSC Discrimination Algorithm

[12] This section describes the PSC discrimination algorithm that we have devised using POAM III PSC observations to discriminate Ia and Ib PSCs. We used a computer model to simulate Type I PSCs formation and radiative effects. A difference in calculated extinction levels and wavelength dependence was observed between Ia and Ib PSCs. We found this difference also existed in POAM III PSC observations in the Northern Hemisphere winter of 1999/2000. Several of the PSCs identified by POAM were verified with coincident lidar measurements.

[13] Radiative extinction caused by atmospheric particles is well described by Mie theory [van de Hulst, 1957]. The extinction of small particles has a strong dependence on wavelength while the extinction of larger particles has a

weak dependence on wavelength. Therefore, given the much larger sizes attributed to Type Ia PSC particles, we expect that their extinction will have a weak wavelength dependence whereas the extinction of the much smaller Type Ib PSC particles should have a relatively strong wavelength dependence. Our approach to discriminating these two types of PSCs is based on this anticipated behavior.

[14] The Integrated MicroPhysics and Aerosol Chemistry on Trajectories (IMPACT) model [Drdla *et al.*, 1996] has been used to simulate PSCs and confirm their radiative behavior. These calculations have focused on idealized cases using IMPACT as a box model in order to determine general relationships between PSC type and radiative characteristics. The IMPACT model simulates the PSC microphysics, heterogeneous chemistry, gas-phase chemistry, and radiative effects of aerosols. The model microphysics calculates the evolution of the multiple particle types that may be present in a PSC, including liquid sulfate aerosols, ternary solutions, heterogeneous nuclei and solid phase Types I and II PSCs. The processes simulated include condensation, evaporation, sedimentation, nucleation, freezing, melting, and radiative extinction.

[15] In all the simulations considered for this paper, the solid phase Type I PSC are assumed to be NAT. This assumption is consistent with SOLVE/THESEO 2000 measurements [Drdla *et al.*, 2002]. To introduce frozen particles, we assumed that a heterogeneous freezing process occurred in which a percentage of the initial sulfate aerosols are assumed to contain an impurity which promotes freezing as soon as the saturation ratio of NAT exceeds 2. The exact composition of the nucleus is not specified. The fraction of particles containing these nuclei has been varied from 0.01 to 0.0001.

[16] Initial gas phase concentrations for H₂O and HNO₃ are 5 ppmv and 10 ppbv, respectively. The initial sulfate distribution used to initialize the model was based on the measured distributions [Wilson *et al.*, 1992]. This initial distribution is shown in Figure 1a. The background aerosol distribution was assumed to be a lognormal distribution with concentration and modal radius of 10 particles per cc and 0.08 micron at 210 K temperature and 50 mbar pressure. The extinction coefficient generated by this distribution was slightly greater than POAM background aerosol observations during SOLVE/THESEO 2000.

[17] In these idealized simulations, the temperature is decreased from 197 K to 188 K in the first 6 days. The saturation temperatures with respect to NAT and ice, T_{NAT} and T_{ICE} , were approximately 196 K and 187 K, respectively. The temperature then remained at 188 K for the remainder of the 10-day simulation. This temperature history was to insure that the particles had ample time to grow and reach equilibrium. The objective here was to compare the growth and properties of STS and NAT particles. Many cases were run to examine the radiative characteristics of clouds produced under different microphysical conditions; five of these are discussed here and their parameters are shown in Table 1. In simulations A and B background sulfuric acid particles were allowed to grow by uptake of nitric acid and water but the freezing mechanism was turned off. This simulated the growth of STS, or Type Ib PSC. A typical STS size distribution is shown in Figure 1a. The

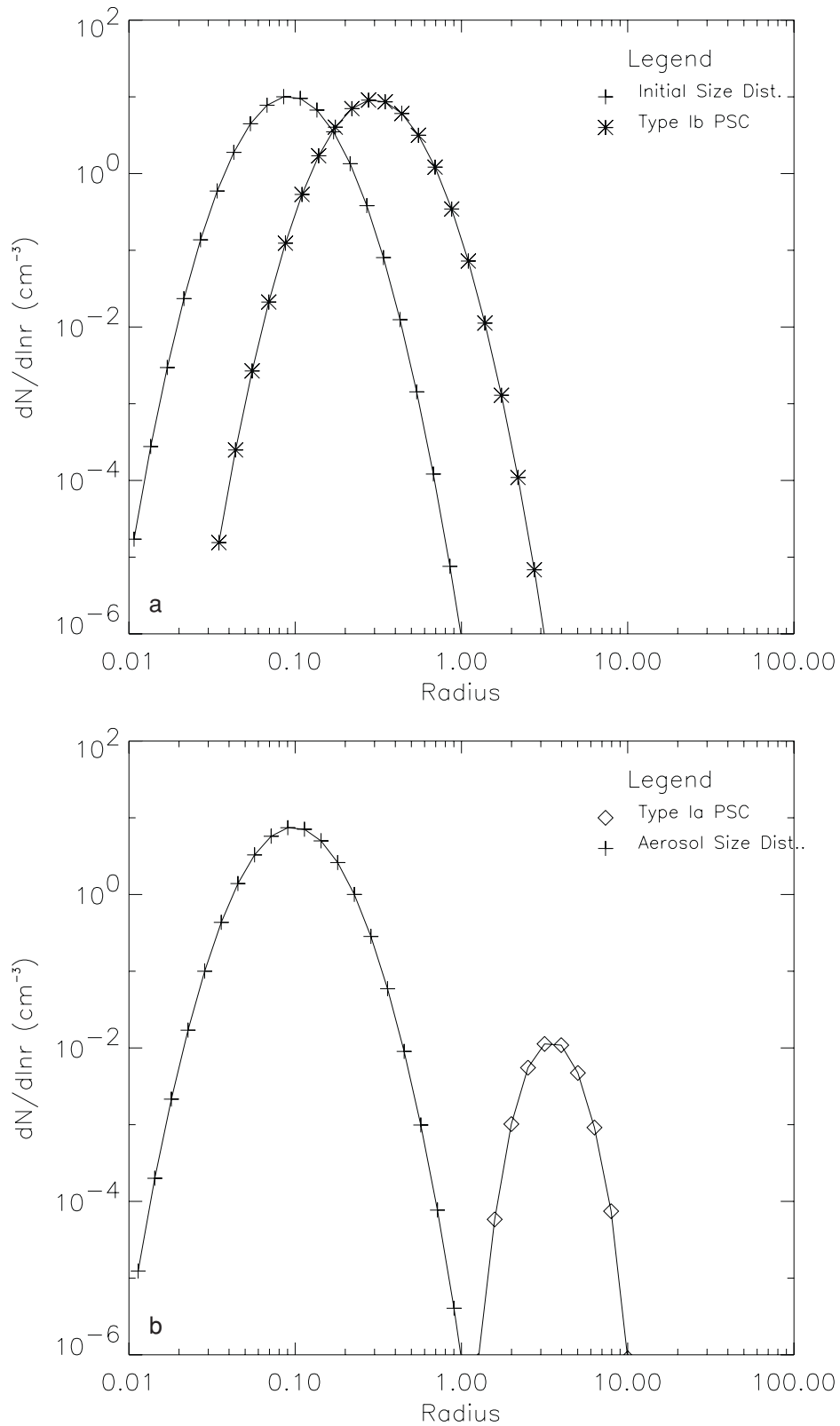


Figure 1. Calculated size distributions for STS and NAT clouds after a 10-day simulation. (a) Initial sulfate aerosol size distribution (pluses), STS size distribution (asterisks). (b) Type Ia size distribution: NAT distribution (diamonds), remaining sulfate aerosol distribution (pluses).

Table 1. Simulation Parameters

Simulation	PSC type	Initial temp, K	Final temp, K	Theta, K	Freezing fraction, —	Initial aerosol number density ^a , no./cc	Initial Aerosol Modal Radius, μm	NO _y , ppbv
A	STS	197	188	460	NA	10	0.08	10
B	STS	197	188	460	NA	25	0.06	10
C	NAT	197	189	460	0.0001	10	0.08	10
D	NAT	197	188	460	0.001	10	0.08	10
E	NAT	197	188	460	0.0001	25	0.06	10
F	STS	205	196	330	NA	10	0.08	2
G	NAT	205	196	330	0.001	10	0.08	2

^aAt T = 210 K and 50 mbar. The actual distribution for any simulation changes the number density to keep the amount of sulfate in this distribution in equilibrium.

modal radius has grown from the initial background value of 0.08 microns to about 0.3 microns. In simulations C, D, and E, a percentage of the liquid aerosol was allowed to freeze. Once freezing started, the particles took up nitric acid quickly and grew into NAT particles within a day. Several freezing fractions were used in the calculations ranging from 0.0001 to 0.01 of the background concentration. The final NAT size distribution for the case of a 0.001 freezing fraction, shown in Figure 1b, produces large NAT particles whose sizes are consistent with recent SOLVE/THESEO 2000 observations of NAT particles, although the concentration is larger [Fahey *et al.*, 2001]. The other distribution in Figure 1b is that of the remaining background aerosol. The NAT modal radius was about 3 μm with sizes extending up to 10 μm and concentration of about 0.001 particles per cc. Figure 2 shows the final extinction coefficient versus wavelength for simulations A and D. Type Ib (STS) has a larger extinction but greater wavelength dependence as expected for a large number of small spherical particles. The extinction curve for the NAT (Type

Ia) PSC is lower but the wavelength dependence is flatter as expected for a small number of solid particles.

[18] We exploit the relationships between the extinction and wavelength dependence of the PSCs to tell them apart in the satellite data. As the particles grew, it was observed that the 1 μm extinction values increased for both NAT and STS, however the wavelength dependence of the extinction differed. The wavelength dependence is represented by the ratio of 1.018 to 0.603 μm extinctions. The ratio of simulated PSC extinction to background extinction at 1 μm (hereafter called ext-bg) is plotted against the wavelength dependence (hereafter called wd) in Figure 3. Simulations A and B correspond to the formation of STS particles (freezing turned off). Onset of particle growth occurred at about 191 K and particle growth was within 90% of equilibrium in less than 1 day. Three simulations show the formation of NAT particles. Ext-bg values are plotted versus wd for freezing rates of 0.001 (Simulation D), and 0.0001 (Simulations C and E), as indicated in the figure caption and in Table 1. The STS and NAT curves bifurcate

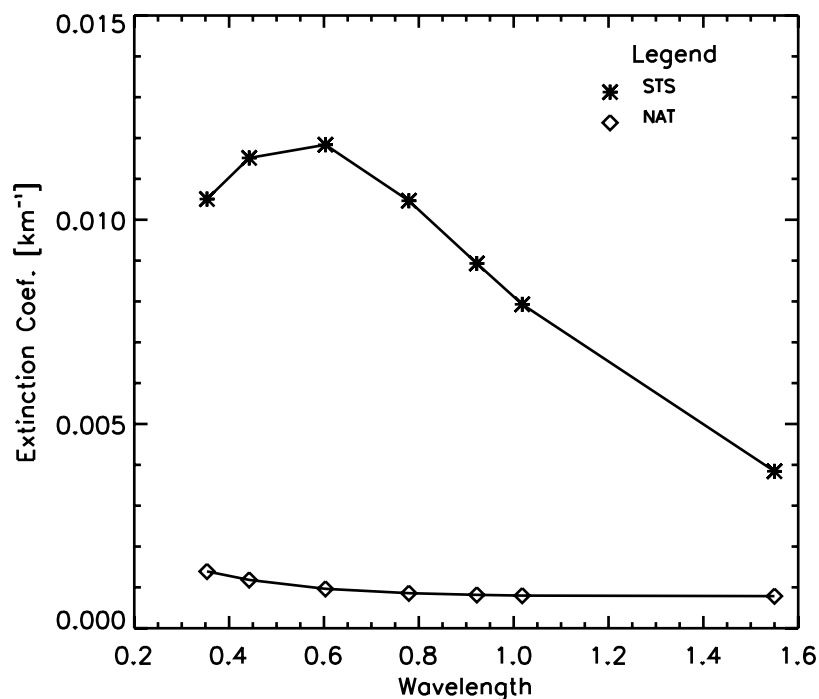


Figure 2. Calculated extinction coefficient versus wavelength for the size distributions presented in Figure 1. STS, asterisks; NAT, diamonds.

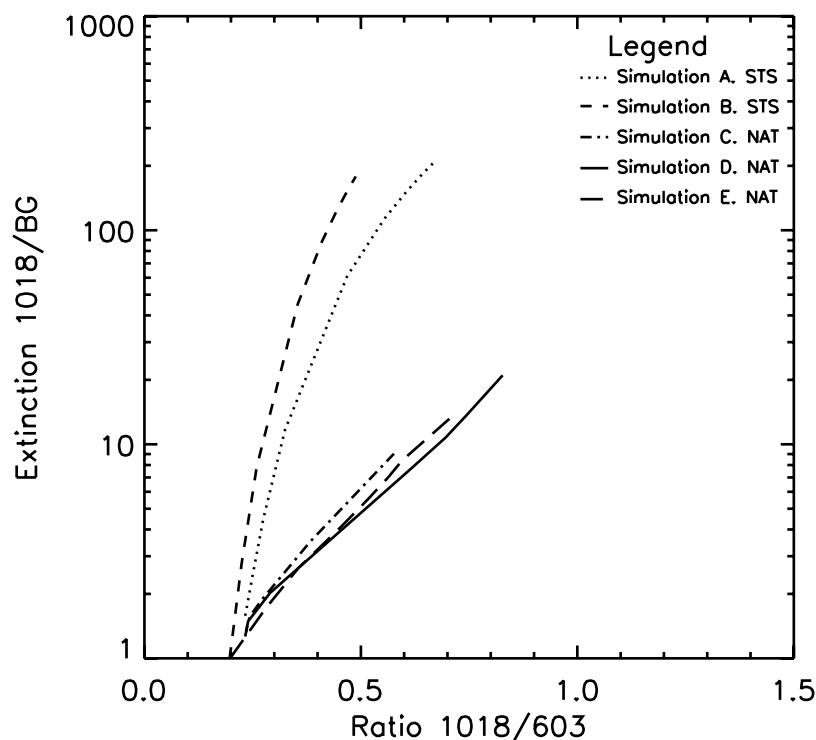


Figure 3. Simulations of the formation of STS and NAT particles. The ordinate is $1\ \mu\text{m}$ extinction coefficient normalized by the background aerosol extinction coefficient. The abscissa is the wavelength dependence (the ratio of $1\ \mu\text{m}$ to $0.6\ \mu\text{m}$ extinction). Pluses represent STS formation (no freezing) with a minimum temperature of 190 K. Asterisks represent STS formation with minimum temperature of 188 K. Open symbols represent the heterogeneous freezing of NAT particles. Diamonds represent a freezing rate, $F = 0.0001$; triangles, $F = 0.001$; squares, $F = 0.01$. As the temperature falls, the particles grow and the extinction increases. The curves for STS and NAT bifurcate at ext-bg equal to about 1.5 where approximately 10% of the available nitric acid has condensed as NAT.

when approximately 10% of the available nitric acid is in the form of NAT. Increased uptake of nitric acid causes the NAT particles to grow large enough to dominate the radiative properties of the size distribution. NAT particle growth started at about 194 K and was essentially complete in 2 days. During this time the surface area density of the NAT particles increases dramatically, from $5 \times 10^{-11}\ \text{cm}^3\text{-cm}^{-3}$ to $1.2 \times 10^{-8}\ \text{cm}^3\text{-cm}^{-3}$. The (wd, ext-bg) values increase from (0.22, 1.0) to (0.82, 20). Similar behavior was observed for all simulations of STS and NAT particles. Changes in the temperature history and water and nitric acid abundance had little effect on the extinction properties of the clouds. The initial size distribution had the greatest effect on the radiative properties of the clouds. This is illustrated by Simulations B and E in which the background size distribution was increased to 25 particles per cc and modal radius was decreased to $0.06\ \mu\text{m}$. The resultant STS simulation curve is seen to shift slightly to smaller wavelength dependence, but there is little effect on the NAT simulation. Altitude has a large effect on PSC radiative properties. The $1\ \mu\text{m}$ extinction coefficient is normalized by the background extinction coefficient to compensate for part of the altitude dependence, but there are two effects that this normalization does not take into account. The abundance of NO_y (and hence HNO_3) increases with increasing altitude, while the abundance of sulfate decreases. Typical values of sulfate and NO_y at 21 km

are 0.1 ppbv and 10 ppbv, respectively, while at 15 km typical values are 0.2 ppbv and 2 ppbv, respectively. Thus the mass increase upon PSC formation is much greater at the higher altitude, which affects directly the change in extinction coefficient for both Ia and Ib PSCs. Simulations of STS and NAT PSCs at 15 km were run to show the effect of changes in the concentration of NO_y ; simultaneous changes in sulfur concentration would magnify the variations. The conditions for simulations F and G are shown in Table 1 and the curves are shown in Figure 4. Plotted for reference are the simulations A and C at 21 km. The simulations appear to tilt toward values of lower ext-bg and higher wd.

4. Results and Discussion

[19] Figure 5 compares POAM PSC observations in the altitude range of 20–21 km compared with simulations made at 21 km. Observations clearly bifurcate in (wd, ext-bg) space. Agreement of the observations with the STS simulation A and NAT simulation C is good although the STS simulation tends to underpredict the wavelength dependence a bit. As mentioned previously, only PSC with the largest extinction coefficient were used in this study. One reason for this is that the motivation of this study is to identify PSCs that can cause denitrification. Clouds with lower values of extinction coefficient likely contain too

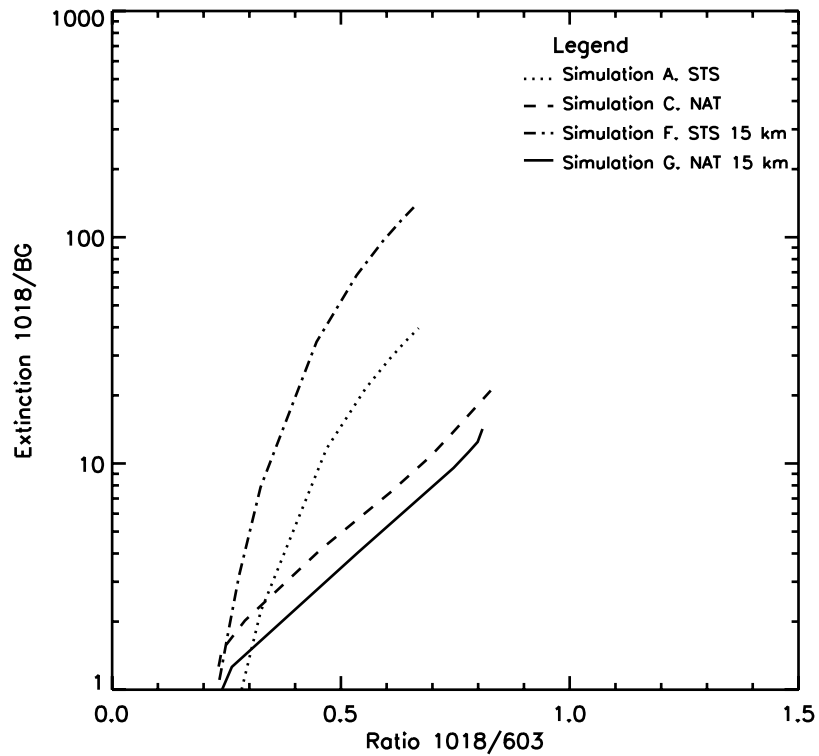


Figure 4. Same as Figure 3 comparing the simulations at 21 km, simulations A and C; with simulations at 15 km, simulations F and G. Parameters are listed in Table 1. The dotted line shows STS at 15 km and the dash-dot-dot-dot line shows NAT at 15 km. Simulations A, dash-dot, for STS at 21 km, and simulation C for NAT at 21 km.

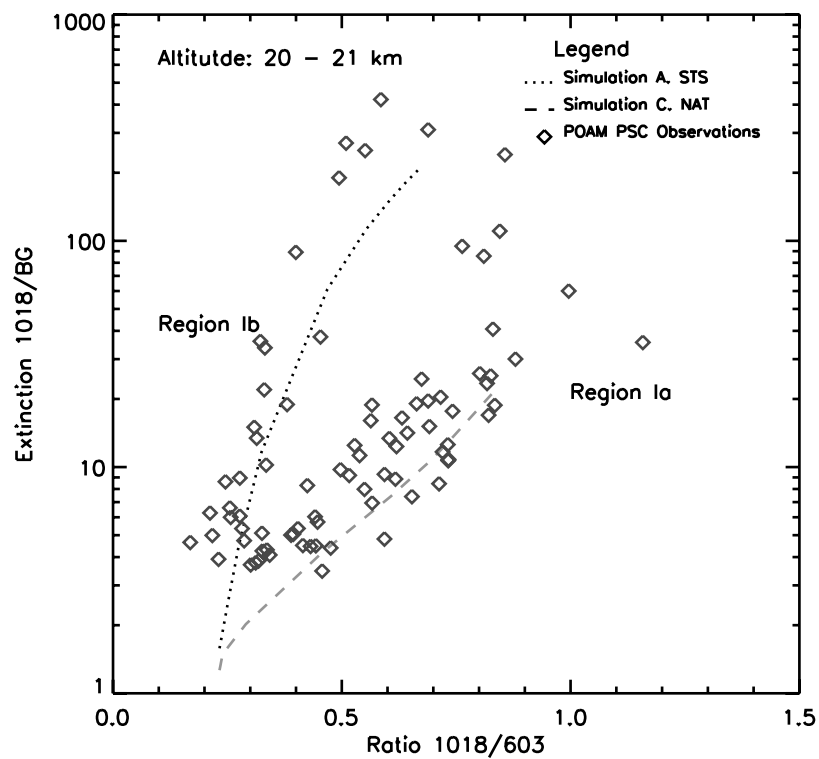


Figure 5. POAM observations of PSCs during the Arctic winter of 1999/2000 between 20 and 21 km altitude, inclusive, plotted as diamonds in (wd, ext-bg) space. Example simulations A and C for STS and NAT are plotted for comparison.

little mass to cause denitrification. The bifurcation of Types Ia and Ib clouds occurs at (wd, ext-bg) of about (0.3, 4.0). There is some scatter to the observations. Typically, the uncertainty in the POAM extinctions is considered to be about 15% [Lumpe, 2002]. The POAM sample volume is typically about 200 km long, 30 km wide, and 1 km thick. In this volume there may be nonhomogeneous clouds, producing scatter in the observations. Clouds that do not fill the entire sample volume would produce a lower value of extinction coefficient. There also appears to be a slight bias to the simulations, with the STS having slightly higher wd ratios and the NAT having slightly larger wd ratios. A larger wd ratio could be caused by too large particles in the simulation. These differences may be due to the assumptions used in the simulations. While changes in the heterogeneous freezing fraction had little effect in these simulations, we did not explore other freezing scenarios in this study. Increasing the number density and decreasing the modal radius of the initial background aerosol (as in Simulations B and E) resulted in shifts in the proper direction although the magnitude of the changes seems excessive. The radiative calculations assumed spherical particles while lidar data demonstrate that Type Ia particles are not spherical.

[20] A cluster of five observations with ext-bg greater than 80 and wd greater than 0.7 appear to lie in an area between Types Ia and Ib simulations. The radiative properties of these clouds are well below the Type II PSC threshold, which is approximately at an ext-bg ratio of 1000. In all simulations, the particles were allowed to come into equilibrium with their surroundings and we were unable to drive the Ia simulations to ext-bg values greater than 20. These may be clouds that contain a mixture of both STS and NAT particles in sufficient numbers that the combined wavelength dependence is averaged. Previous researchers have also observed mixed clouds [Toon *et al.*, 2000] (E. V. Browell *et al.*, Polar stratospheric cloud types, distributions, optical characteristics, and correlations with temperatures and gravity waves during the SOLVE campaign, submitted to *Journal of Geophysical Research*, July 2001, hereinafter referred to as Browell *et al.*, submitted manuscript, 2001). Several simulations, not presented here, resulted in mixed clouds with properties similar to the observations that existed for short periods of time during the simulations. A more rigorous study of this question will be taken up in the future. Despite these factors, the generally excellent agreement between simulations and observations in Figure 5 encourages a confident discrimination between STS and NAT clouds using this method.

[21] A criterion for discriminating Types Ia and Ib clouds was selected midway between Ia and Ib groups of observations guided by the simulations and POAM PSC observations at 20–21 km. The criterion is described by a line of the form

$$\text{Ext} - \text{BG} = \exp(A * \text{WD} - 1.5) \quad (1)$$

where A is a coefficient equal to 8.5 in this altitude range. The y axis intercept was chosen based on the fact that in the simulations the background aerosol always had a wavelength dependence of 0.22. Of course the ext-bg value for the background aerosol was always 1.

[22] POAM PSC observations for the 1999/2000 Northern Hemisphere winter are plotted in (wd, ext-bg) space for six altitude bins in Figure 6. As was observed with the simulation results shown in Figure 4, the observations tilt toward lower ext-bg and higher wd as the altitude decreases. The theoretical simulations and the observations give us the confidence to include this altitude dependence in the criterion. This altitude variation was captured reasonably well by changing the coefficient A by 0.8 per 2 km bin. Thus the coefficient for the 24–25 km was 10.1; 22–23 km, 9.3; 20–21 km, 8.5; 18–19 km, 7.7; 16–17 km, 6.9; 14–15 km, 6.1. The criterion lines are shown as solid in Figure 6. It is also worth noting that the ratio of the 1 μm extinction coefficient to the background extinction coefficient generally decreases with altitude.

[23] Uncertainty in the 1 μm extinction coefficient is estimated to be 15% [Lumpe, 2002]. While no estimate for the 603 nm extinction coefficient is available, it is reasonable to estimate this at 15% also. The background extinction coefficient was averaged over 10 to 14 points, so its uncertainty is about a factor of three less than that of the other extinction coefficients or about 5%. Analysis of the uncertainties associated with each observation is complicated by the fact that the 1 mm extinction coefficient appears in the numerator of the quantities on both axes in Figure 6. Estimates of the combined uncertainty for ext-bg and wd were computed using a random number generator, based on the uncertainties listed above for each extinction observation. If the observation and its uncertainty lay entirely on either side of the criterion line then the observation was classified as a Type Ia or Ib. If any part of the uncertainty associated with the observation crossed the criterion line, it was considered an undetermined PSC Type. The uncertainty envelope on either side the criterion line is approximated by dashed lines in Figure 6. The undetermined observations are represented by crosses in Figure 6, while the observations classified as Type Ia or Ib are represented by diamonds. Observations that lie to the left of the criterion line and outside of the uncertainty envelope, in Region Ib, are considered to be Type Ib or STS clouds, and observations that lie to the right of the line and outside of the uncertainty envelope, in Region Ia, are considered to be Type Ia or NAT clouds. This conservative approach was adopted to make the discrimination method more robust.

[24] Several other observations, located in a region of low ext-bg and high wd, were also eliminated from the analysis. These are discussed below. They are classified as undetermined for this study because they lie well outside the group of observations that can clearly be identified as Type Ia PSCs and because we were unable to generate points in that region of the graph in any of our simulations. These points are also represented by crosses in Figure 6.

[25] A statistical analysis was carried out in order to give confidence that the criterion selected above could faithfully discriminate between Types Ia and Ib PSCs. The criterion for each altitude bin was used to separate the observations into Type Ia, Type Ib and undetermined groups. Then linear regressions were fit through the Ia and Ib observations and the following questions were posed about the pair of each regression in each altitude bin: (1) Is the slope of regression line statistically significant? That is, is it different from a line with zero slope? (2) Are the two regressions statistically

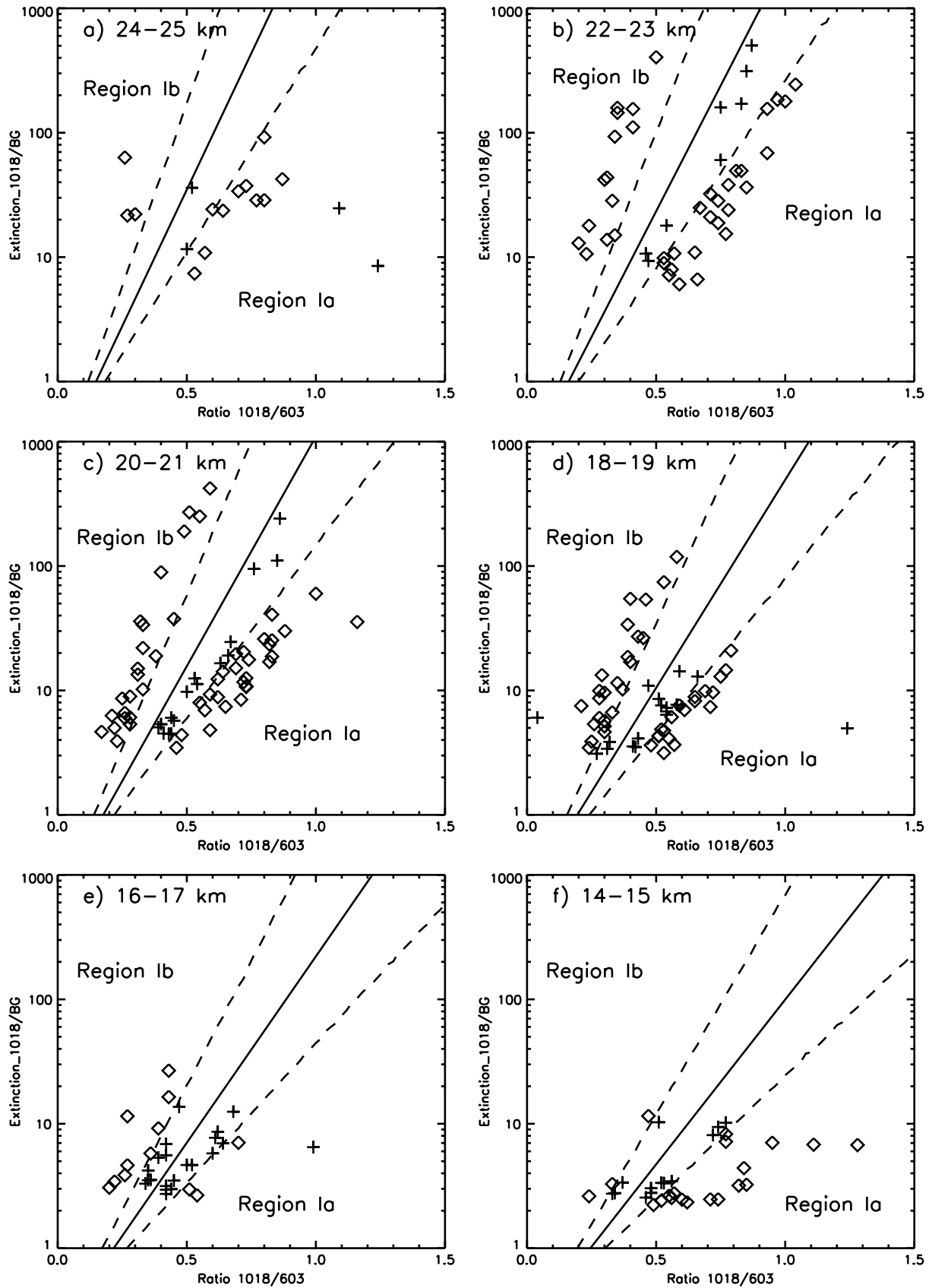


Figure 6. POAM observations of PSCs during the Arctic winter of 1999/2000 between 15 and 25 km altitude plotted in (wd, ext-bg) space: (a) 24–25 km (there were no PSC observations above 26 km), (b) 22–23 km, (c) 20–21 km, (d) 18–19 km, (e) 16–17 km, and (f) 14–15 km. The criterion discussed in the text is displayed.

Table 2. PSC Discrimination Criteria for Lidar Data^a

PSC type	Composition	IR-scattering	IR-depolarization	Wavelength dependence
Ia	NAT/NAD	2–5	20–50%	0–1
Ib	STS	5–20	<4%	2–3
II	water ice	>20	>10%	<0.8

^aFrom *Browell et al.*'s [1990] study.

different from each other? (3) If the regressions (i.e., slope and/or intercept) differ significantly, are the slopes of the two lines different from one another? The first two statistical questions were answered by applying *F* test statistics and the third was answered by applying a *t*-test. Of the twelve regression lines tested in this way, most met of the above criteria with at least 95% confidence. The three exceptions were the cases in which there were only three observations in the population. However, since all of the other cases were statistically significant, it is reasonable to assume that these cases would be also, given more observations.

[26] Other criteria for the discrimination of Types Ia and Ib PSCs different from the one chosen in this study are possible. For example, an envelope of allowed values around the STS and NAT simulation lines could be developed. However, the criteria chosen has the advantages of capturing the essential features of the simulations and observations and of being easily implemented.

[27] Further confidence in the validity of the method is obtained by comparing POAM PSC observations with the DIAL lidar (*Browell et al.*, submitted manuscript, 2001), which was flown on the DC-8 and OLEX [*Dörnbrack et al.*, 2002] flown aboard the DLR Falcon during SOLVE/THESEO 2000. Eight lidar observations of PSCs were found to be coincident with POAM observations of PSCs. For the purposes of this analysis we defined coincidence to be where the longitude of the aircraft observation nearly aligned with the back or forward trajectory of the POAM observation. Latitudinal distances are limited to within ±100 km. This corresponds to the POAM III line-of-sight and

sample volume (about 200 km along the line-of-sight). The difference in time between POAM observation and aircraft coincidence was limited to several hours, but, temperature histories were examined to insure that the temperature did not change dramatically within this period. Selection criteria used for determining Types Ia and Ib PSCs from the lidar data are shown in Table 2 and are taken from *Browell et al.*'s [1990] data. Of the eight coincident observations, four were classified as Type Ib by both the present analysis of POAM observations and the lidars. (These are identified by POAM revolution number (REV) 9545, 9573, 9574, and 9559.) The four other observations were identified as Type Ia PSCs by both the lidar and the discrimination algorithm. (These points are identified REV 9516, 9544, 9473, and 9415.) Table 3 lists the POAM III and lidar observations that led to the PSC determination. Note that agreement was found for all eight cases. The observation at REV 9415 actually has an extinction coefficient lower than the 4-sigma threshold used to filter out weak PSCs mentioned earlier. The fact that both the lidar and the present analysis scheme classify this observation as a Type Ia PSCs demonstrates that the 4-sigma requirement is very conservative. This requirement could have been relaxed somewhat and still maintain the integrity of the method.

[28] As previously mentioned, several points on Figure 6 are of interest because they lie well to the right of the criterion line. Two of these points, (0.99, 6.48) and (1.24, 4.96), belong to REV 9544 on 25 January 2000, at 69 N, 28.8 W, and at adjacent altitudes, 17 and 18 km. PSCs are also observed at this REV at altitudes up to 23 km. Both the 1 mm extinction profile and wavelength dependence show three distinct layers of PSCs, one between 21 and 23 km, another between 17 and 18 km, both identified as Type Ia separated by a layer of Type Ib. The DIAL lidar observes a similar profile in this region of the atmosphere at about the same time. A sparse population of large particles would have ext-bg versus wd characteristics similar to those observed at 17 and 18 km. It is possible then that this may be an observation of NAT particles that have been

Table 3. DC-8 DIAL/POAM Coincidence During SOLVE/THESEO 2000

Date		16 January 2000	20 January 2000	23 January 2000	25 January 2000	25 January 2000	26 January 2000	27 January 2000	27 January 2000
POAM	REV	9415	9473	9516	9544	9545	9559	9573	9574
	Obs. time	1049	1255	1337	1258	1439	1420	1400	1541
	Latitude	55.55	26.75	17.97	29.07	3.75	9.33	14.92	349.60
	PSC alt	19	20	22	22	22	23	20	18
	Ext/BG ^a	2.8	23.44	184.5	68.7	15.0	27.6	8.95	26.43
	WD1	0.49	0.82	0.97	0.93	0.34	0.46	0.28	0.45
	POAM PSC type	Ia	Ia	Ia	Ia	Ib	Ib	Ib	Ib
DIAL	Coin. time	1020	0852	1242	0801	1439	–	1420	1542
	IR_backscat	0.5–1.5	1–5	5–20	10	2–10	–	2–10	1–7
	IR_depolar	20	20–30	30–50	20–40	0–10	–	0–15	0
	WD	1–1.5	<0.5	<1	<0.1	1.5	–	>1	1.5
	DIAL PSC type	Ia	Ia	Ia	Ia	Ib	–	Ib	Ib
OLEX ^b	Coin. time						1439		
	OLEX PSC type						Ib		

^aExt/BG is the ratio of 1 μm extinction to background extinction; wavelength dependence (WD) is the ratio of 1 μm to 0.6 μm extinction. NB. The WD derived from POAM cannot be directly compared to the WD derived from the lidar.

^bSee *Dörnbrack et al.* [2002, Figure 9] reference.

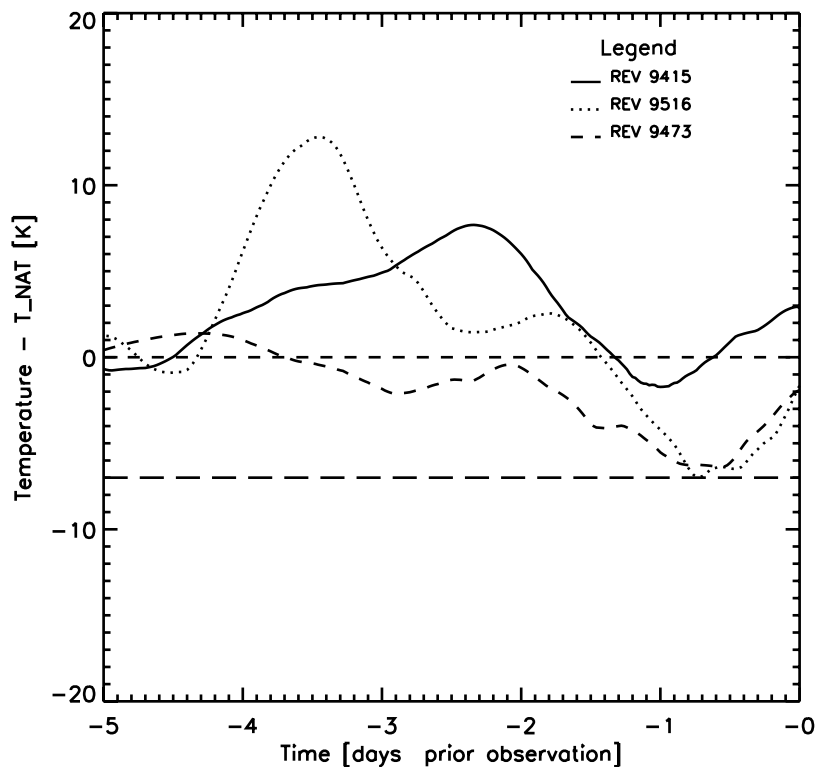


Figure 7. Five-day UKMO temperature backtrajectories for three POAM Type Ia observations plotted as $T - T_{\text{NAT}}$ versus time prior to observation: REV 9415, solid; REV 9516, dotted; REV 9473, dashed. The ice frost point is shown as a dashed line at -7 K.

sedimented from higher altitudes. PSCs observed at 13 and 14 km in March, not included in the present data set, have low values of ext-bg and high values of wd, similar to the points under consideration. This lends further support to the hypothesis that these clouds represent particles that have sedimented from higher altitudes. Another possible explanation for these observations is that only a portion of the POAM observing volume contained the PSC. The POAM observing volume is approximately 200 km long by 30 km wide by 1 km high. If a PSC was present in only a portion of the sample volume width, the wavelength dependence observed by POAM would be the same as a Type Ia PSC but the $1 \mu\text{m}$ extinction would be reduced, bringing these observations into the region of interest. At present the formation mechanism of these PSCs is unknown and requires further study.

[29] Three POAM Type Ia observations are explored in more detail using backtrajectory analysis. Figure 7 shows 5-day United Kingdom Meteorology Office (UKMO) temperature histories plotted as $T - T_{\text{NAT}}$ versus days prior to the observation. T_{NAT} is calculated for each point in the backtrajectory assuming concentrations of 5 ppmv and 10 ppbv for water vapor and nitric acid, respectively. Rev 9415 has a (wd, ext-bg) equal to (0.5, 2.8) and is located near the criterion envelope in Figure 6e. Rev 9473 (0.82, 23.4) and Rev 9516 (0.97, 184.5) are in Figures 6c and 6b, respectively. These observations were chosen because each of them are identified as Ia clouds using the present method and from the DIAL lidar data. REV 9415 is the weakest of the PSCs and its temperature history just dips below T_{NAT} the day before the observation and is actually 3 K above

T_{NAT} at the time of the observation. REVs 9473 and 9516 show very similar temperature histories despite the fact that REV 9516 has considerable stronger extinction. It is difficult to explain these observations based on their temperature histories. There is much uncertainty about the mechanisms responsible for NAT nucleation and evolution. Studies showing that NAT form only after prolonged exposure below the NAT saturation temperature, T_{NAT} , suggest a homogeneous nucleation mechanism. However, many of the backtrajectories for Type Ia PSC observations by POAM show periods below T_{NAT} of only 1 day. To date no single theory can explain all of the available data. Several studies have pointed out that in some cases the temperatures derived from the assimilated models may be biased to warmer temperatures and this possibility must be considered. It is worth noting that typically, T_{NAT} is calculated assuming values for the nitric acid and water vapor mixing ratios, which are generally not known. The values used in this study are 10 ppbv and 5 ppmv for nitric acid and water vapor, respectively. An error in either of these quantities can have an effect on the calculated NAT frost point. For example, changing the water vapor mixing ratio from 5 to 6 ppmv can increase T_{NAT} by as much as one degree.

[30] Results from the discrimination algorithm that was used on the POAM PSC observations for the Arctic winter of 1999/2000 are tabulated in Table 4. As mentioned previously, only the strongest PSCs were considered in this study. Of the 328 PSC observations, 32% were identified as Type Ia, 23% as Type Ib, and 45% as undetermined over the course of the winter. The large number of undetermined PSCs is the result of the very conservative criterion used.

Table 4. Frequency and Partitioning of Type I PSC Observations for Arctic Winter 1999/2000

	November	December	January	February	March	Total
Total PSC observations	10	42	174	38	64	328
POAM Type Ia (%)	30	58	37	18	9	32
POAM Type Ib (%)	10	21	16	48	33	23
POAM undetermined (%)	60	21	47	34	58	45
DIAL Type Ia (% vert. area)	–	93.6	39.5	–	40.6	–
DIAL Type Ib (% vert. area)	–	0	16.6	–	41.2	–

Figure 8a shows a histogram of Types Ia and Ib PSC observations. The number of PSCs observed reached a peak in January and the percentage of Type Ia PSCs was greatest in December and January. In February and March, the percentage of Type Ib PSCs was higher. Winter temperatures dropped below T_{NAT} in November over a limited region reflected by the relatively few strong PSC observation in that month. Temperatures dropped below T_{NAT} over a progressively larger region in December, January, and

February [Bevilacqua et al., 2002]. The large number of strong PSC observations indicates that a large percentage of vortex air was processed by PSCs during this period. Furthermore, this analysis shows that a large percentage of these PSCs were Type Ia, consisting of large particles capable of sedimentation and denitrification. This is consistent with other observations made during SOLVE/THESEO 2000. Fahey et al. [2001] observed large particles containing a large amount of nitric acid and evidence of the

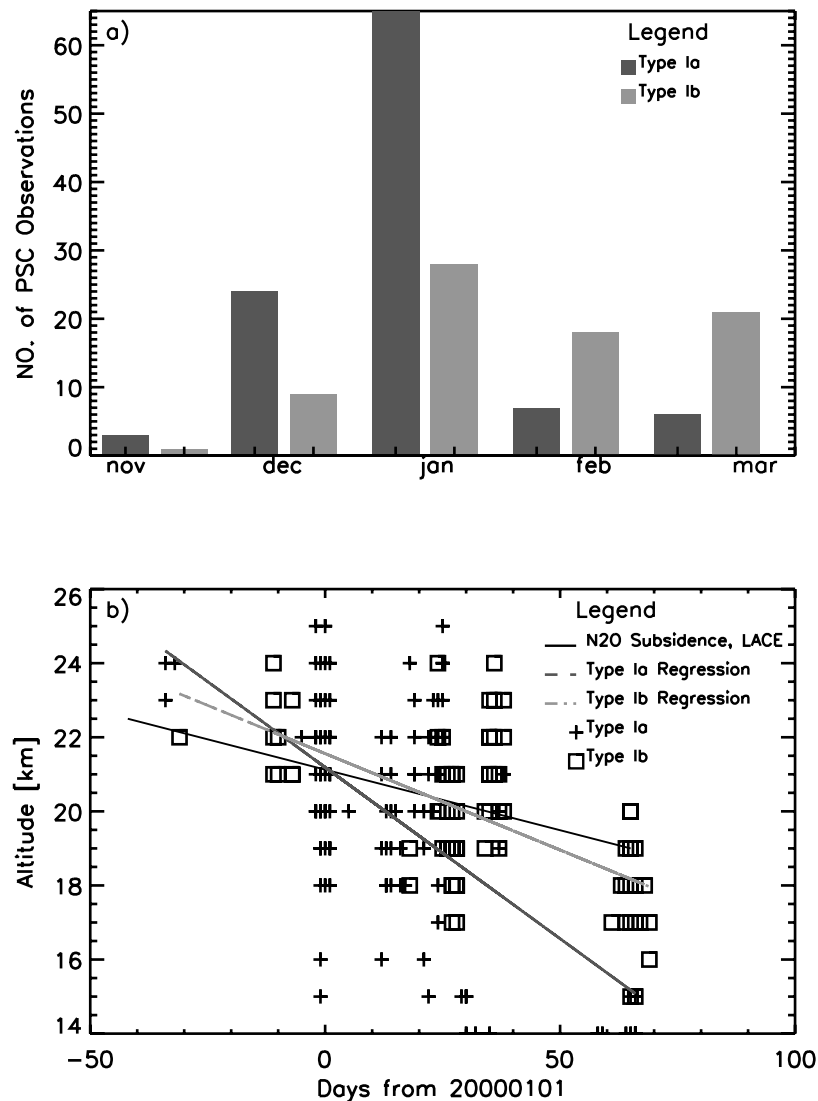


Figure 8. (a) Distribution of POAM PSC Ia and Ib observations over the course of the 1999/2000 Arctic winter. (b) Altitude of POAM PSC observations plotted versus day beginning with 1 January 2000.

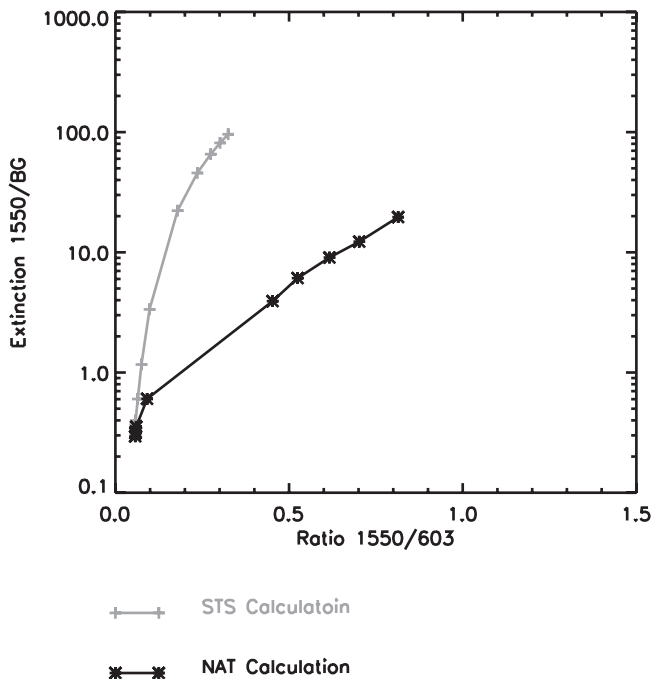


Figure 9. Simulations A and C of STS and NAT plotted in (wd, ext-bg) space simulating the wavelengths of the SAGE III instrument. The ordinate is 1.55 mm extinction coefficient normalized by the background aerosol extinction coefficient. The abscissa is the wavelength dependence (the ratio of 1.55 μm to 0.6 μm extinction).

occurrence of denitrification with measurement made aboard the ER-2 aircraft. Denitrification during this period has also been observed with MLS (Microwave Limb Sounder) satellite measurements [Santee *et al.*, 2000]. While the cold pool was still large in February, it was situated inside of the POAM observation region which at this time were in a band circumnavigating the pole at about 67° latitude. Thus the number of PSC observations in February is low. In mid-March, the vortex began to break up. The last POAM PSC observation was on 15 March. However, there are still 64 PSC observations in this month.

[31] The ratio of Type Ia to Ib observations in November, December, and January is 3, 2.7, and 2.3, respectively. This ratio reverses in February and March to 0.38 and 0.28. To explore this observation further, Figure 8b shows the distribution of PSC observations in altitude over the course of the 1999/2000 Arctic winter broken into Types Ia and Ib. For clarity, linear regressions for the data are also shown on the plot. As the winter progresses Type Ia PSCs are observed at increasingly lower altitudes than Type Ib. For comparison, the subsidence of stratospheric air is represented by the altitude decrease of a tracer gas, N_2O , as measured by the LACE experiment on board a balloon at the beginning and end of the 1999/2000 Arctic winter (F. L. Moore *et al.*, First in situ gas chromatograph on a balloon platform yielding tracer measurements with improved spatial resolution: Description and intercomparison, in preparation). As the winter progresses, observations of Type Ib PSCs tend to occur at lower altitudes than the tracer measurements would indicate for the descent of the air mass. PSC formation, however is governed primarily by the

temperature of the air mass and there is evidence that the center of the cold pool descended more rapidly than the subsidence [Drda *et al.*, 2002]. The descent of the Type Ib PSC observations follows the descent of the cold pool. The regressions were subjected to an f-statistics analysis and show that Type Ia PSCs are more likely to be observed at lower altitudes than the Type Ib PSCs as the winter progresses by a statistically significant margin. Both are observed at about the same average altitude in December and early January but in February and March the average altitude of Type Ia observations is 2–3 km lower. This coincides with the reversal of the Ia to Ib ratio. Presently, the reasons for this are unclear. Denitrification was observed during this winter after January above 16 km and not below 16 km [Popp *et al.*, 2001]. This however, cannot explain the change in the ratio of Type Ia to Ib PSCs after January since denitrification would suppress Types Ia and Ib cloud formation by about the same amount. One possibility is that the concentration of nuclei needed for the heterogeneous formation of Ia PSCs has been depleted at the higher altitudes during the course of the winter. In other words, Type Ia PSCs sediment to lower altitudes during the winter, taking with them the nuclei responsible for their formation. When they reach lower stratospheric altitudes, below the cold pool, they evaporate and deposit their nuclei. Later in the winter, there are too few nuclei for Type Ia formation and Type Ib formation is favored at the higher altitudes. This would also account for the change in the ratio of Type Ia to Ib PSCs observed in February and March.

[32] The percentage of in-vortex clouds identified as Types Ia and Ib by the DIAL lidar during the SOLVE/THESEO 2000 deployment are also shown in Table 4 for comparison with the results of this method. The DC-8 data show 93.6% of the PSC vertical area (defined as altitude times flight path distance) are identified as Type Ia in December, 39.5% in January, and 40% in March compared to 58%, 37%, and 28% for the present method. The ratio of Ia to Ib lidar observations is 130 in December, 2.3 in January, and 1.0 in March. The reasons for the very large percentage of Ia lidar observations in December compared to the POAM observations is perhaps explained by sampling differences between the two instruments. As mentioned previously, POAM observations are made 14 times a day approximately along a band of latitude between 61 and 68 North. The DC-8 on the other hand has the ability to fly under the cold pool. During December the cold pool rarely reached POAM observation latitudes. The January ratio, however, is consistent with the ratio of the present method. While the ratio in March goes down there are more Ia lidar observations than seen with the present method. Yet, the general trend in both observation sets is consistent: Ias make up a very large percentage of observations in December and January, but in March the occurrences of Ias have dropped considerably. Differences between the POAM and lidar observations are to be expected and are attributable in part to sampling differences between the two instruments. PSCs were observed on only two of the DC-8 flights in March, whereas POAM made 25 observations of PSCs in the vortex. Keeping in mind that the POAM observations reported here are all within the vortex, the discrepancy between the partitioning of Types Ia and Ib PSCs for DC-8 and POAM underscores the fact that the cold pool only makes up a fraction of the vortex. These

sampling differences must be considered when comparing observations from different instruments.

5. Conclusions

[33] A method for discriminating Types Ia and Ib PSCs from POAM satellite occultation measurements of aerosol extinction has been presented. The method has been validated by applying several statistical tests to the results and by using DIAL and OLEX lidar measurements made during SOLVE/THESEO 2000. The significance of this method is that Type Ia PSCs are believed to be composed of large nitric-acid-containing particles that will sediment out of the stratosphere causing denitrification. A decrease in the concentration of nitric acid allows chlorine to remain in its active forms longer and results in increased ozone depletion. Type Ib PSCs are believed to be much smaller and will not sediment out of the stratosphere. Therefore identifying Type Ia PSC events may provide information on when and where denitrification is occurring. Satellite occultation data provide more continuous temporal coverage and larger areal coverage than the lidar data, which has been used to date to identify Types Ia and Ib PSCs. One drawback is that satellite occultation measurements are usually confined to latitudes less than about 70° .

[34] The method is made possible by the character of POAM observations when plotted as normalized extinction versus wavelength dependence. As the extinction increases, observations of Types Ia and Ib PSCs bifurcate on a plot of ext/bg versus wd as the wavelength dependence of the Type Ia PSCs increases. This behavior was also observed in simulations of the formation of STS and NAT particles.

[35] Analysis of POAM observations from the 1999/2000 Arctic winter using the PSC discrimination algorithm revealed that both the number of PSC observations and the percentage of Type Ia PSCs peaked in January. In November, December, and January, the ratio of Type Ia to Ib PSCs was about 3, while in February and March it was about 0.3. During December and early January, Types Ia and Ib PSCs were observed at about the same altitude. In February and March, however, the altitude of the Type Ia observations was below that of the Type Ib observations by 2–3 km. These changes coincide with denitrification, which was observed in the Arctic stratosphere during SOLVE/THESEO 2000 from both aircraft and satellites. Establishing a linkage between satellite observations of Type Ia PSCs and stratospheric denitrification will be the focus of future work using this method.

[36] Unfortunately SAGE III was not launched in time to be a part of the SOLVE/THESEO 2000 mission. It is logical, however, to extend the present analysis to determine the capability of SAGE III to discriminate between Types Ia and Ib PSCs, since SAGE III includes an aerosol wavelength at $1.55 \mu\text{m}$. The results of this analysis applied at SAGE III wavelengths is shown in Figure 9. It is seen that the SAGE III wavelength at $1.55 \mu\text{m}$ is even more effective than the $1.018 \mu\text{m}$ wavelength for discriminating Type Ia from Type Ib clouds. It is our belief that the present method of analyzing satellite data to discriminate Type I PSCs will be of great utility in the study of PSCs and ozone depletion.

[37] The PSC discrimination algorithm is applicable to previous winters, and will work with future SAGE III

observations as well. This will permit a more extensive study of the statistical significance of some features of the PSCs observed during the 1999/2000 Arctic winter. In the future the PSC discrimination algorithm will be used to study PSC observations from previous winters in both hemispheres. We will look for evidence linking satellite observations of Type Ia PSCs and denitrification events, establish a Type Ia climatology as observed by satellite observations, and investigate interhemispheric and interannual variability. To date the simulations of PSC formation have been used as a guide to establishing the criteria outlined in this paper. In the future we will use our modeling capability to make a more exhaustive study of the parameter space used by this method. It is our belief that the present method of analyzing satellite data to discriminate Type I PSCs will be of great utility in the study of PSCs and ozone depletion.

[38] **Acknowledgments.** The authors wish to acknowledge the support of NASA's Upper Atmosphere Research and Atmospheric Chemistry Modeling and Analysis Programs.

References

- Bevilacqua, R. M., et al., Observations and analysis of polar stratospheric clouds detected by POAM III during the 1999/2000 Northern Hemisphere winter, *J. Geophys. Res.*, *107*, doi:10.1029/2001JD000477, in press, 2002.
- Browell, et al., Airborne LIDAR observations in the wintertime Arctic stratosphere, *Geophys. Res. Lett.*, *17*, 385–388, 1990.
- Del Negro, L. A., et al., Evaluating the role of NAT, NAD, and liquid $\text{H}_2\text{SO}_4/\text{H}_2\text{O}/\text{HNO}_3$ solutions in Antarctic PSC aerosol: Observation and implications, *J. Geophys. Res.*, *102*, 13,255, 1997.
- Dörnbrack, A., T. Birner, A. Fix, H. Flentje, A. Miester, H. Schmid, E. V. Browell, and M. J. Mahoney, Evidence for inertia-gravity waves forming polar stratospheric clouds over Scandinavia, *J. Geophys. Res.*, in press, 2002.
- Drdla, K., et al., Analysis of the physical state of one Arctic PSC based on observations, *Geophys. Res. Lett.*, *21*, 2475–2478, 1994.
- Drdla, K., et al., Applications of a model of polar stratospheric clouds and heterogeneous chemistry, PhD Thesis, Univ. of Cali., Los Angeles, 1996.
- Drdla, K., M. R. Schoeberl, and E. V. Browell, Microphysical modelling of the 1999–2000 Arctic winter, 1, Polar stratospheric clouds, denitrification, and dehydration, *J. Geophys. Res.*, *107*, doi:10.1029/2001JD000782, in press, 2002.
- Dye, J. E., et al., In situ observations of an Antarctic PSC, *Geophys. Res. Lett.*, *23*, 1913–1916, 1996.
- Fahey, D. W., et al., Observations of denitrification and dehydration in the winter polar stratosphere, *Nature*, *344*, 321–324, 1990.
- Fahey, D. W., et al., The detection of large HNO_3 -containing particles in the winter Arctic stratosphere, *Science*, *291*, 1026–1031, 2001.
- Fromm, M. D., et al., Observations of Antarctic polar stratospheric clouds by POAM II: 1994–1996, *J. Geophys. Res.*, *102*, 23,659–23,672, 1997.
- Fromm, M., et al., An analysis of POAM II Arctic polar stratospheric cloud observations, 1993–1996, *J. Geophys. Res.*, *102*, 23,659–23,672, 1999.
- Goodman, J., S. Verma, R. F. Pueschel, P. Hamill, G. V. Ferry, and D. Webster, New evidence of size and composition of polar stratospheric cloud particles, *Geophys. Res. Lett.*, *25*, 5615–5618, 1997.
- Hanson, D., and M. Mauersberger, Laboratory studies of the nitric acid trihydrate: Implications for the south polar stratosphere, *Geophys. Res. Lett.*, *15*, 855–858, 1988.
- Liou, K. N., *Radiation and Cloud Processes in the Atmosphere*, Oxford Univ. Press, New York, 1992.
- Lou, P. B., T. Peter, and P. J. Crutzen, Freezing of stratospheric aerosol droplets, *Geophys. Res. Lett.*, *21*, 1447–1450, 1994.
- Lucke, R. L., et al., The polar ozone and aerosol measurement (POAM) III instrument and early validation studies, *J. Geophys. Res.*, *104*, 18,785–18,800, 1999.
- Lumpe, R. L., Comparison of POAM III ozone measurements with correlative aircraft and balloon data during SOLVE, *J. Geophys. Res.*, in press, 2002.
- McCormick, M. P., et al., PSC sightings by SAM II, *J. Atmos. Sci.*, *39*, 1387–1397, 1982.
- Mishchenko, M. I., Light scattering by size-shape distributions of randomly

- oriented axially symmetric particles of a size comparable to a wavelength, *Appl. Opt.*, 32(24), 4652–4666, 1993.
- Moore, F. L., et al., Balloon-borne in situ gas chromatography for measurements in the troposphere and stratosphere, *J. Geophys. Res.*, 107, doi:10.1029/2001JD000891, in press, 1992.
- Nash, E. R., et al., An objective determination of the polar vortex using Ertel's potential vorticity, *J. Geophys. Res.*, 101, 9471–9478, 1996.
- Palmer, K. F., and D. Williams, Optical constants of sulfuric acid: Application to the clouds of Venus, *Appl. Opt.*, 14(1), 208–219, 1975.
- Popp, P. J., et al., Severe and extensive denitrification in the 1999–2000 Arctic winter stratosphere, *Geophys. Res. Lett.*, 28, 2875–2878, 2001.
- Rosen, J. M., et al., Simultaneous ozone and PSC observations at south pole station during winter and spring 1991, *J. Geophys. Res.*, 98, 12,741–12,751, 1993.
- Russel, P. B., et al., Global to microscale evolution of the Pinatubo volcanic aerosol, derived from diverse measurements and analyses, *J. Geophys. Res.*, 101, 18,745–18,763, 1996.
- Santee, M. L., et al., Six years of UARS Microwave Limb Sounder HNO₃ observations, *J. Geophys. Res.*, 104, 8225–8246, 1999.
- Santee, M. L., G. L. Manney, N. J. Livesey, and J. W. Waters, UAR Microwave Limb Sounder observations of denitrification and ozone loss in the 2000 Arctic late winter, *Geophys. Res. Lett.*, 27, 3213–3216, 2000.
- Schlager, et al., Balloon observations of nitric acid aerosol formation in the Arctic stratosphere, 1, Gaseous nitric acid, *Geophys. Res. Lett.*, 17, 1275–1278, 1990.
- Steele, H. M., and P. Hamill, Effects of temperature and humidity on the growth and optical properties of sulphuric acid-water droplets in the stratosphere, *J. Aerosol Sci.*, 12, 517–528, 1981.
- Steele, H. M., K. Drdla, R. P. Turco, J. D. Lumpe, and R. M. Bevilacqua, Tracking polar stratospheric cloud development with POAM II and a microphysical model, *Geophys. Res. Lett.*, 26, 287–290, 1999.
- Tolbert, M. A., and O. B. Toon, Solving the PSC mystery, *Science*, 292, 61, 2001.
- Toon, O. B., et al., An analysis of lidar observations of PSCs, *Geophys. Res. Lett.*, 17, 393–396, 1990.
- Toon, O. B., et al., Analysis of lidar observations of Arctic polar stratospheric clouds during January 1989, *J. Geophys. Res.*, 105, 20,589–20,615, 2000.
- Turco, R. P., et al., Heterogeneous physiochemistry of the polar ozone hole, *J. Geophys. Res.*, 94, 16,493–16,510, 1989.
- van de Hulst, H. C., *Light Scattering by Small Particles*, Dover, Mineola, N. Y., 1957.
- Wilson, J. C., M. R. Stolzenburg, W. E. Clark, M. Loewenstein, G. V. Ferry, and K. R. Chan, Stratospheric sulfate aerosol in and near the Northern Hemisphere polar vortex: The morphology of the sulfate layer, *J. Geophys. Res.*, 97, 7997–8013, 1992.
- Worsnop, D. R., et al., Vapor pressure of solid hydrates of nitric acid: Implications for PSCs, *Science*, 259, 71–74, 1993.
-
- E. V. Browell, NASA Langley Research Center, Hampton, VA 23666, USA.
- D. P. Dempsey, Department of Meteorology, San Francisco State University, San Francisco, CA 94132, USA.
- K. Drdla, R. F. Pueschel, and A. W. Strawa, NASA Ames Research Center, Moffett Field, CA 94035, USA. (astrawa@mail.arc.nasa.gov)
- M. Fromm, Computational Physics, Inc., Springfield, VA 22151, USA.
- P. Hamill, Department of Physics, San Jose State University, San Jose, CA 95192, USA.
- K. W. Hoppel, Naval Research Laboratory, Washington, DC 20375, USA.